

PAPER

## Spin reorientation in antiferromagnetic $\text{Dy}_2\text{FeCoO}_6$ double perovskite

To cite this article: G R Haripriya *et al* 2020 *J. Phys.: Condens. Matter* **33** 025802

View the [article online](#) for updates and enhancements.









**IOP | ebooks™**

Bringing together innovative digital publishing with leading authors from the global scientific community.

Start exploring the collection—download the first chapter of every title for free.

# Spin reorientation in antiferromagnetic $\text{Dy}_2\text{FeCoO}_6$ double perovskite

G R Haripriya<sup>1</sup> , T W Heitmann<sup>2</sup>, D K Yadav<sup>3</sup>, G C Kaphle<sup>3,4</sup>, Madhav Prasad Ghimire<sup>3,4,5</sup> , R Pradheesh<sup>1,6</sup>, J Joshi<sup>7,8</sup>, P Vora<sup>7,8</sup> , K Sethupathi<sup>1</sup> , V Sankaranarayanan<sup>1</sup>  and H S Nair<sup>9</sup> 

<sup>1</sup> Low Temperature Physics Laboratory, Department of Physics, Indian Institute of Technology Madras, Chennai-600036, India

<sup>2</sup> University of Missouri Research Reactor, University of Missouri, Columbia, MO 65211, United States of America

<sup>3</sup> Central Department of Physics, Tribhuvan University, Kirtipur, 44613 Kathmandu, Nepal

<sup>4</sup> Condensed Matter Physics Research Center (CMPRC), Butwal-11, Rupandehi, Lumbini, Nepal

<sup>5</sup> IFW Dresden, Helmholtzstr. 20, D-01069, Dresden, Germany

<sup>6</sup> Racah Institute of Physics, Hebrew University of Jerusalem, Jerusalem 91904, Israel

<sup>7</sup> Department of Physics and Astronomy, George Mason University, Fairfax, VA 22030, United States of America

<sup>8</sup> Quantum Materials Center, George Mason University, Fairfax, VA 22030, United States of America

<sup>9</sup> Department of Physics, 500 W University Ave, University of Texas at El Paso, El Paso, TX 79968, United States of America

E-mail: [vsu@physics.iitm.ac.in](mailto:vsu@physics.iitm.ac.in), [ksethu@iitm.ac.in](mailto:ksethu@iitm.ac.in), [h.nair.kris@gmail.com](mailto:h.nair.kris@gmail.com), [hair@utep.edu](mailto:hair@utep.edu) and [madhav.ghimire@cdp.tu.edu.np](mailto:madhav.ghimire@cdp.tu.edu.np)

Received 11 April 2020, revised 16 June 2020

Accepted for publication 12 August 2020

Published 13 October 2020



CrossMark

## Abstract

We explored the electronic and magnetic properties of the lanthanide double perovskite  $\text{Dy}_2\text{FeCoO}_6$  by combining magnetization, Raman and Mössbauer spectroscopy and neutron diffraction along with density functional theory (DFT) calculations. Our magnetization measurements revealed two magnetic phase transitions in  $\text{Dy}_2\text{FeCoO}_6$ . First, a paramagnetic to antiferromagnetic transition at  $T_N = 248$  K and subsequently, a spin reorientation transition at  $T_{SR} = 86$  K. In addition, a field-induced magnetic phase transition with a critical field of  $H_c \approx 20$  kOe is seen at 2 K. Neutron diffraction data suggested cation-disordered orthorhombic structure for  $\text{Dy}_2\text{FeCoO}_6$  in  $Pnma$  space group which is supported by Raman scattering results. The magnetic structures ascertained through representational analysis indicate that at  $T_N$ , a paramagnetic state is transformed to  $\Gamma_5(Cx, Fy, Az)$  antiferromagnetic structure while, at  $T_{SR}$ , Fe/Co moments undergo a spin reorientation to  $\Gamma_3(Gx, Ay, Fz)$ . The refined magnetic moment of (Fe/Co) is  $1.47(4) \mu_B$  at 7 K. The antiferromagnetic structure found experimentally is supported through the DFT calculations which predict an insulating electronic state in  $\text{Dy}_2\text{FeCoO}_6$ .

Keywords: spin reorientation, double perovskite, antiferromagnetism

 Supplementary material for this article is available [online](#)

(Some figures may appear in colour only in the online journal)

## 1. Introduction

Scientific interest in double perovskites stem from the technical possibilities of realizing applications ranging from multiferroics [1, 2] to strongly correlated magnets [3] to solid oxide fuel cells [4] to room temperature magnetoresistive oxides [5]. There is immense interest in obtaining an alternating (ordered) arrangement of  $3d$  and  $5d$  cations as a route to combine strong electronic correlations of  $3d$  ions with the spin–orbit coupling of  $5d$  whereby exotic magnetism and spin–orbit-assisted Mott insulating state was recently observed in  $\text{Ca}_2\text{MnReO}_6$  [6]. Potential Mott multiferroics are identified recently in polar materials like  $\text{A}_2\text{VFeO}_6$  which is a solid solution of non-ferroelectric  $\text{AVO}_3$  and  $\text{AFeO}_3$  ( $A = \text{Ba}, \text{Pb}$  etc) [7]. The possibility of achieving favorable ferroelectric or multiferroic properties through the combination of non-polar or non-ferroelectric components is a motivating concept to explore many more double perovskite structures with emergent properties. The perovskite  $\text{DyFeO}_3$  belongs to the family of orthoferrites that crystallize in the orthorhombic  $Pnma$  structure and has attracted attention in recent times due to the discovery of a magnetic field induced ferroelectric state at low temperature [8]. The experimental discovery of magnetoelectric effect by Tokunaga *et al*, [8] was supported subsequently by *ab initio* density functional theory (DFT) calculations [9]. A ferroelectric state was observed at very low temperature where the Dy moments start to order,  $T_N^{\text{Dy}} = 3.5$  K [8]. A linear magnetoelectric tensor component,  $\alpha_{zz} \approx 2.4 \times 10^{-2}$  esu, which induced a ferroelectric polarization along the crystallographic  $c$ -axis was experimentally determined in the case of  $\text{DyFeO}_3$ . Both the experimental work and the DFT calculations argue that the origin of the ferroelectric polarization in the multiferroic state is due to the exchange striction effect between adjacent  $\text{Fe}^{3+}$  and  $\text{Dy}^{3+}$  layers with antiferromagnetic exchange. In addition, the DFT studies suggested that the interaction between the  $f$  and the  $d$  sublattices might be used to tailor the multiferroic properties of this orthoferrite. The Fe sublattice in  $\text{DyFeO}_3$  orders at significantly higher temperature,  $T_N^{\text{Fe}} = 645$  K [9].

On the other hand, the orthoperovskite compound  $\text{DyCoO}_3$  adopts  $Pnma$  structure but orders magnetically at very low temperature,  $T_N = 3.6$  K [10]. The magnetic properties are dominated by Dy in this compound where  $\text{Co}^{3+}$  remains in a non-magnetic, low-spin state. Noncollinear magnetic structures are formed by the Dy moments which carry Ising character. Structural anomalies are observed in  $\text{DyCoO}_3$  at high temperatures where the orthorhombic distortion parameter displays an anomaly [11]. Solid solutions of  $\text{RFeO}_3$  and  $\text{RCoO}_3$  ( $R$  is a rare earth) were studied in the case of  $R = \text{La}$  for  $\text{LaCo}_{1-x}\text{Fe}_x\text{O}_3$  [12]. The compositions for which  $x > 0.5$  were reported to show weak ferromagnetism with a  $G_z$  component of antiferromagnetism. The magnetism of the solid solution was found to be governed by the low-spin state of  $\text{Co}^{3+}$ . However, detailed studies on solid solutions of  $\text{RFeO}_3$  and  $\text{RCoO}_3$  forming double perovskite structures are limited. Many of the Fe/Co double perovskites are computationally predicted to be ferromagnetic semiconductors, for example  $\text{La}_2\text{FeCoO}_6$  [13, 14]. Such ferromagnetic materials are prime candidates for

spintronics applications. A preliminary account of the crystal structure and the magnetic properties of several  $\text{R}_2\text{FeCoO}_6$  has been reported by some of us [15]. In the present paper we compile the results of magnetic measurements, crystal and magnetic structure determined through neutron diffraction and DFT studies of electronic and magnetic properties of  $\text{Dy}_2\text{FeCoO}_6$ . Our results reveal spin re-orientation transitions present in this insulating, antiferromagnetic double perovskite. Our results on  $\text{Dy}_2\text{FeCoO}_6$  will be interesting to materials research in double perovskites searching for Mott insulators and multiferroics for novel applications.

## 2. Experimental techniques

Polycrystalline powders of  $\text{Dy}_2\text{FeCoO}_6$  used in the present study were prepared by citrate based sol–gel method. Details of the synthesis can be found elsewhere [15]. Phase purity and crystal structure of the sample were verified using powder x-ray diffraction patterns taken at 300 K (PAN’Alytical, XPert Pro) using  $\text{Cu-K}\alpha$  radiation with a wavelength of  $1.5406$  Å. Mössbauer spectra was recorded with  $\text{Co}^{57}$  source, in transmission mode using a standard PC based Mössbauer spectrometer (UGC-DAE CSR, Indore). DC and AC magnetization measurements were carried out on pelleted samples of  $\text{Dy}_2\text{FeCoO}_6$  using a commercial SQUID based vibrating sample magnetometer (SVSM, Quantum Design Inc., USA). About 3–4 g powder sample was used for neutron powder diffraction experiments at the PSD instrument at the University of Missouri Research Reactor. Neutrons of wavelength  $1.485$  Å were used in the experiment. Neutron diffraction patterns were recorded at 300 K, 150 K and 7 K in order to investigate the nuclear and magnetic structures of  $\text{Dy}_2\text{FeCoO}_6$ . The order parameter as represented by the intensity of the (011) peak was measured on the TRIAX triple axis spectrometer. The diffraction data were analyzed using the Rietveld method [16] as coded in the FullProf suite of programs [17]. For the determination of the magnetic structure, the software SARA $h$  was used which employs representation analysis method [18]. The structural diagrams presented in this paper were prepared using the software VESTA [19]. Low and high-temperature Raman measurements were carried out on a home-built confocal microscope setup with 532 nm ( $2.4$  μm spot size;  $<500$  μW laser power measured pre-objective) and 50x long working distance objective. The light is collected in a back-scattering geometry, with the collection fiber-coupled to a 500 mm focal length single spectrometer integrated with a liquid-N $_2$  cooled CCD detector. The sample was placed under vacuum and cooled in a closed-cycle He cryostat with a variable temperature range from 5 K to 300 K. Excitation laser polarization is kept constant for all measurements unless otherwise noted.

## 3. Computational methods

The DFT calculations have been considered using the full-potential linearized augmented plane wave method as implemented in the WIEN2K code [20]. The non overlapping

muffin-tin sphere radii ( $R_{MT}$ ) were fixed at 2.32, 1.98, 1.98 and 1.70 Bohr radii for Dy, Fe, Co, and O, respectively. The linear tetrahedron method with 1000  $k$  points ( $10 \times 8 \times 11$   $k$  mesh) was employed for the reciprocal-space integrations in the whole Brillouin zone (BZ). This corresponds to 442  $k$ -points within the irreducible BZ. In the initial calculations, the standard generalized-gradient approximation (GGA) in the parameterization of Perdew, Burke, and Ernzerhof (PBE-96) was used [21]. In order to consider the strong correlation effects, the GGA +  $U$  functional with double-counting corrections according to Anisimov *et al* [22] was used. The chosen values of  $U$  are 7 eV for Dy-4 $f$ , 3 eV for Co-3 $d$ , and 5 eV for Fe-3 $d$  states, which are comparable to the values found in the literature [23–29]. Spin–orbit coupling (SOC) was considered through a second variational step using the scalar relativistic eigenfunctions as basis [30]. The calculations were performed by using the experimental lattice parameters obtained at 7 K from the neutron diffraction experiments reported in the present work. The energy and charge convergence for the self-consistent calculations was set to  $10^{-5}$  Ry and  $10^{-4}$  of an electron respectively. Magnetic ground states were obtained by computing the total energies for different magnetic configurations.

## 4. Results and discussion

### 4.1. Magnetization and Mössbauer

The temperature-dependent magnetization curves,  $M(T)$ , of  $\text{Dy}_2\text{FeCoO}_6$  in the ZFC mode obtained under external magnetic field values of 100 Oe, 500 Oe, 1 kOe, 5 kOe, 10 kOe, 20 kOe, 50 kOe and 70 kOe are shown in figure 1(a). The data were recorded during the warming cycle of the measurement. A magnetic anomaly is present at low applied magnetic fields (for magnetic fields below 20 kOe) at  $\approx 248$  K which we assign here as the  $T_N$ . The  $M(T)$  curves show a second anomaly at  $\approx 86$  K in measuring fields  $H_{app}$  up to 20 kOe, which gets suppressed by higher magnetic fields. The anomaly at 86 K ( $T_{SR}$ ) is identified as the spin re-orientation transition similar to that in  $\text{DyFeO}_3$  [31]. This is in agreement with the earlier reports on  $\text{Dy}_2\text{FeCoO}_6$  by some of us [15, 32]. In the case of  $\text{DyFeO}_3$ ,  $T_N = 645$  K and  $T_{SR}$  is in the range of 50–75 K and a  $T_{N2} = 4.5$  K is also identified [31]. The  $T_N$  and the  $T_{SR}$  correspond to the magnetic transitions in the Fe sublattice whereas the  $T_{N2}$  corresponds to the transition in the Dy lattice. In the present case of  $\text{Dy}_2\text{FeCoO}_6$ , the  $T_N$  is reduced from 645 K to 248 K while  $T_{SR}$  is at 86 K. There is no sign of  $T_{N2}$  down to 5 K in the present case.

As the applied magnetic field increases, the peak features at  $T_N$  and  $T_{SR}$  are reduced in strength and vanish completely at 70 kOe.  $\text{Dy}_2\text{FeCoO}_6$  shows irreversibility between the zero field cooled and the field cooled magnetization curves, in additions to strong thermal hysteresis between the cooling and warming cycles of the field cooled magnetization [15]. The irreversibility and thermal hysteresis could arise from several factors including a slow spin dynamics where one magnetic structure transforms into another, disorder effects related to cation occupation which is common in double perovskites, or

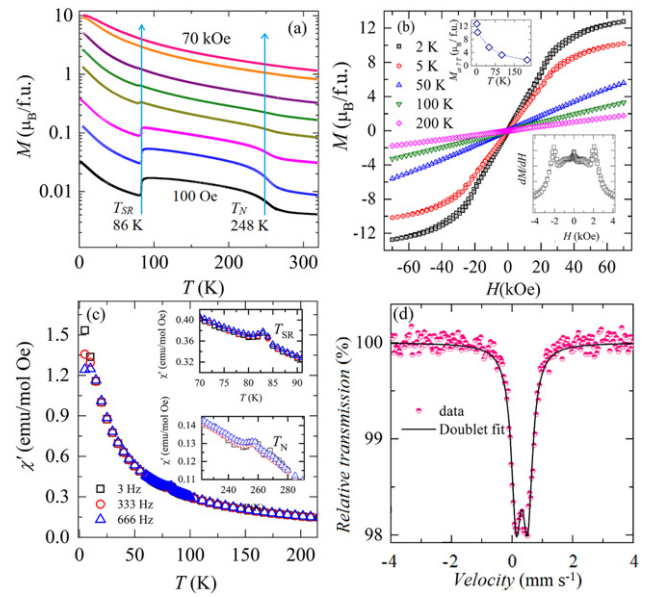


**Figure 1.** (a) The DC magnetization versus temperature curves of  $\text{Dy}_2\text{FeCoO}_6$  in ZFC mode with different measuring magnetic fields 100 Oe, 500 Oe, 1 kOe, 5 kOe, 10 kOe, 20 kOe, 50 kOe and 70 kOe. Magnetic anomalies are present at  $T_N$  and  $T_{SR}$  which are marked in the figure. (b) Isothermal magnetization curves at 2 K, 5 K, 50 K, 100 K and 200 K. The inset on the top (lhs) represents the plot of the maximum moment value obtained at each temperature for the magnetic field of 70 kOe vs respective temperatures. The inset on the bottom (rhs) shows the derivative,  $dM/dH$ , in which field-induced metamagnetic transitions are evident for the 2 K data. (c) The real part of AC susceptibility ( $\chi'(T)$ ) at 3 Hz, 333 Hz and 666 Hz. The top and bottom insets magnify the region around  $T_{SR}$  and  $T_N$  respectively. (d) The Mössbauer spectra of  $\text{Dy}_2\text{FeCoO}_6$  obtained at room temperature. The raw data is represented by pink top-closed circles. The solid line is a fit using a Lorentzian line shape for a doublet.

spin glass effects. The magnetic susceptibility of  $\text{Dy}_2\text{FeCoO}_6$  is analyzed using modified Curie–Weiss law,  $\chi(T) = \chi_0 + C/(T - T_C)$ , to obtain the Curie–Weiss temperature  $\theta_p = +65(1)$  K and effective paramagnetic moment  $\mu_{eff} = 12.49 \mu_B$  (fit not shown).

The isothermal magnetization curves of  $\text{Dy}_2\text{FeCoO}_6$  at different temperatures are shown in figure 1(b). The magnetic moment value attained by  $\text{Dy}_2\text{FeCoO}_6$  at 2 K, 70 kOe is  $\mu_{max} = 12.7 \mu_B$ . The 5 K isothermal data shows  $\mu_{max} = 10.19 \mu_B$  for the magnetic field value 70 kOe. A metamagnetic transition is present at 2 K, which is clearer in the derivative plot shown in the inset of (b). The critical field,  $H_c = \pm 20$  kOe is identified from the derivative plot,  $dM/dT$ . The inset on the top (lhs) of panel (b) represents the variation of maximum magnetic moment (at 70 kOe) with temperature. At  $T > 5$  K, the magnetization isotherms are representative of a paramagnetic-like spin system.

Figure 1(c) shows the real part of AC susceptibility for the frequencies 3 Hz, 333 Hz and 666 Hz. Peaks at  $T_N$  and  $T_{SR}$  are clearly observed in the AC susceptibility response. The inset of panel (c) magnifies the region around  $T_N$  and  $T_{SR}$ . There is no frequency dependence to either peaks in the measured frequency window, which rules out spin dynamics related to spin-glass like physics. A weak inflection is observed at low



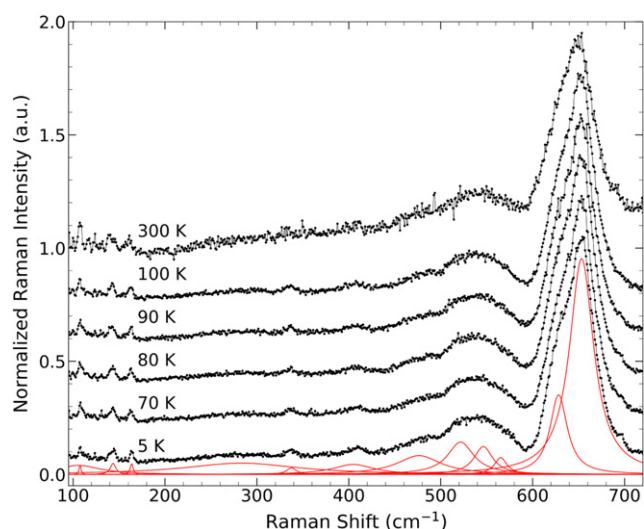


**Figure 2.** The Raman intensity of  $\text{Dy}_2\text{FeCoO}_6$  as a function of wave numbers at different temperatures. The red curves are the Lorentzians used to identify vibrational modes. Spectra are normalized by maximum intensity.

temperatures close to 2 K which might be due to the magnetism stemming from Dy. The DFT calculations presented in a later section offer an explanation to this observation.

The oxidation state of Fe in  $\text{Dy}_2\text{FeCoO}_6$  was determined using Mössbauer spectroscopy data taken in transmission mode, see figure 1(d). The room temperature spectrum is deconvoluted into a doublet using the software Fit'O; [33]. In the figure, a fit to the experimental Mössbauer data using a Lorentzian doublet is shown in solid black line. From the fit, the quadrupole splitting and the isomer shift values are estimated as  $\Delta E_Q = 0.37(4) \text{ mm s}^{-1}$  and  $\delta = 0.32(4) \text{ mm s}^{-1}$  respectively. The observed value of quadrupole shift point towards the existence of a significant charge asymmetry around  $\text{Fe}^{3+}$  [34–36].

#### 4.2. Raman scattering

Temperature-dependent Raman spectra of  $\text{Dy}_2\text{FeCoO}_6$  is presented in figure 2. Mode frequencies are extracted from the 5 K data by fitting with a sum of 13 Lorentzians (red curves in the figure). The observed spectra are consistent with the assigned *Pnma* orthorhombic crystal symmetry based on prior studies on perovskite systems [37–43]. With increasing temperature we observe only minimal changes to the spectra, which implies that the system remains in the *Pnma* structural phase. The spectra are dominated at all temperatures by two prominent modes appearing at  $\sim 630$  and  $\sim 650 \text{ cm}^{-1}$ . These features are common in double perovskites and are thought to originate from oxygen breathing and stretching modes of the *B*-site octahedra [37–39, 41]. The observed modes can be assigned an origin in Co or Fe compounds based on prior studies of the perovskites  $\text{DyFeO}_3$  [37] and  $\text{DyCoO}_3$  [38]. The weak intensity of modes below  $600 \text{ cm}^{-1}$  is curious as perovskites typically exhibit strong, sharp modes in this range [37–39, 41]. In contrast, double perovskites often exhibit suppressed intensity in this range [41, 43]. Studies on Ho and La based compounds

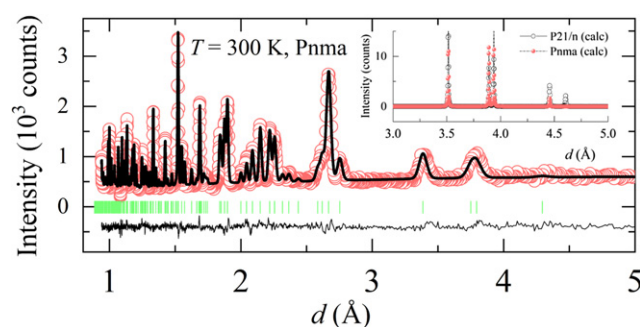


**Figure 3.** The neutron diffraction pattern of  $\text{Dy}_2\text{FeCoO}_6$  at 300 K shown in red circles and the Rietveld fits using *Pnma* structure model in black. The inset shows an overlay of calculated neutron diffraction patterns of *Pnma* and  $P2_1/n$  structures of  $\text{Dy}_2\text{FeCoO}_6$ . The samples used in the present study conform to the orthorhombic structure.

have attributed the enhancement of the  $\sim 650 \text{ cm}^{-1}$  modes to charge transfer between the *B* site atoms that in turn activates oxygen breathing modes [39, 44] although octahedral tilt and structural changes also likely contribute [41, 44].

#### 4.3. Neutron diffraction

The neutron diffraction pattern of  $\text{Dy}_2\text{FeCoO}_6$  at 300 K is presented in figure 3(a) using circles as markers. Double perovskites often adopt a cation-ordered structure if they crystallize in monoclinic  $P2_1/n$  space group, or a cation-disordered structure in *Pnma*. In the case of  $P2_1/n$ , the Fe and Co atoms in  $\text{Dy}_2\text{FeCoO}_6$  will occupy distinct Wyckoff positions,  $2c(0, \frac{1}{2}, 0)$  and  $2d(\frac{1}{2}, 0, 0)$ . In the present case of  $\text{Dy}_2\text{FeCoO}_6$ , Rietveld fits to the data using  $P2_1/n$  and *Pnma* gave comparable goodness-of-fit values (2.6 and 2.4 respectively) and visual fit quality. The room temperature synchrotron x-ray diffraction data of  $\text{Dy}_2\text{FeCoO}_6$  reported by some of us, had the best fit for the mixed system *Pbnm* (29.57%) +  $P2_1/n$  (70.43%), where *Pbnm* is an alternative setting of *Pnma* [15]. High degree of cation order at the  $2c$  and  $2d$  Wyckoff positions, as per the monoclinic space group, will result in significant intensity for the (011) Bragg peak [45]. In the case of  $\text{La}_2\text{MnCoO}_6$ , a high degree of ordering between Mn and Co was achieved as a result of controlled synthesis methods where 95% order was obtained for the ordered version of  $\text{La}_2\text{MnCoO}_6$  whereas 74% for the disordered [45]. The absence of an intense (011)-peak in the case of  $\text{Dy}_2\text{FeCoO}_6$  suggests a disordered cation arrangement pertaining to the orthorhombic *Pnma* structure. Hence, the nuclear structure of the current compound was refined in *Pnma*.

From a comparison of the calculated neutron diffraction patterns of the ordered (monoclinic) and disordered (orthorhombic) structures for  $\text{Dy}_2\text{FeCoO}_6$ , a better match is seen for the orthorhombic structure. Thus, Rietveld refinements were performed using the *Pnma* space group model. The results of the refinement and the comparison of calculated neutron diffraction patterns of *Pnma* and  $P2_1/n$  are shown in figure 3. The bond valence sums (BVS) were estimated from the bond parameters after the refinement of

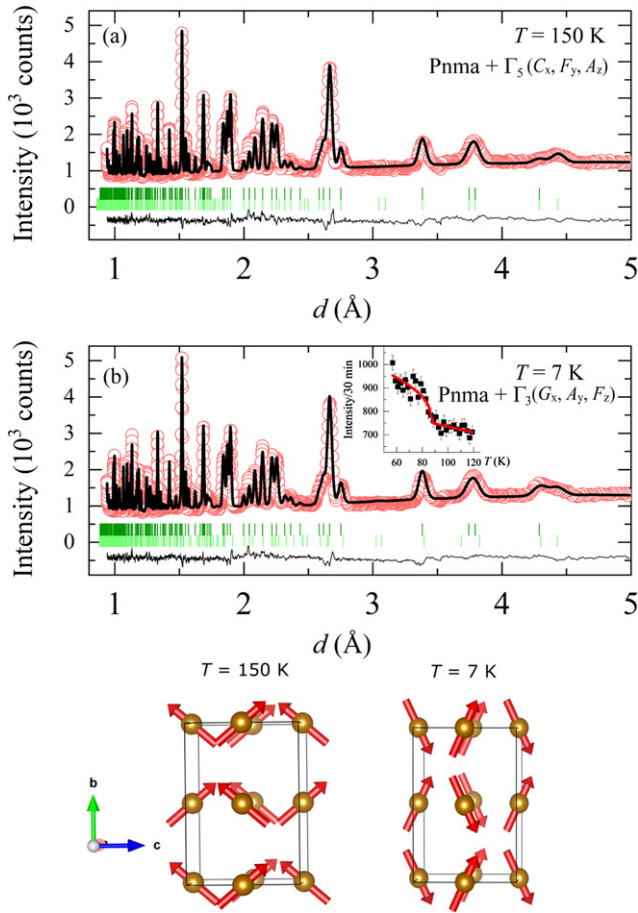


**Figure 4.** The neutron diffraction pattern of  $\text{Dy}_2\text{FeCoO}_6$  at (a) 150 K and (b) 7 K. The nuclear structure remains in orthorhombic space group while the magnetic structure transforms from  $\Gamma_5(Cx, Fy, Az)$  at 150 K to  $\Gamma_3(Gx, Ay, Fz)$  at 7 K. The inset of (b) shows the variation of intensity of (011) Bragg peak as a function of temperature along with a power-law fit which confirms the  $T_{\text{SR}}$ . The magnetic structures of  $\text{Dy}_2\text{FeCoO}_6$  above (at  $T = 150$  K) and below (at  $T = 7$  K) the  $T_{\text{SR}}$  are shown.

crystal structure using neutron diffraction data. The BondStr utility in FullProf was used for this purpose. The average bond length in the transition metal polyhedra (1.973(2) Å) matched well with the BVS estimates of  $\text{Co}^{3+}$  (1.956(3) Å),  $\text{Fe}^{3+}$  (2.032 Å) and  $\text{Fe}^{4+}$  (1.915 Å). This supports the presence of mixed valent states for Fe/Co in  $\text{Dy}_2\text{FeCoO}_6$  in orthorhombic structure.

As the temperature is reduced from 300 K,  $\text{Dy}_2\text{FeCoO}_6$  undergoes a magnetic phase transition at  $T_N = 248$  K (see figure 1(a)). Figure 4(a) shows the neutron diffraction pattern of  $\text{Dy}_2\text{FeCoO}_6$  at 150 K. There are no additional Bragg peaks at this temperature when compared to the pattern at 300 K, but only enhancement of intensity for the nuclear Bragg peaks, and hence the same nuclear model used for 300 K ( $Pnma$ ) was retained. In order to determine the magnetic structure of  $\text{Dy}_2\text{FeCoO}_6$  at 150 K, the magnetic propagation vector was determined as (000) using the  $k$ -search utility in FullProf. Subsequently, the magnetic structure was solved using the representation analysis method coded in SARA $h$ . Symmetry analysis suggested four magnetic representations,  $\Gamma_1(Ax, Gy, Cz)$ ,

**Table 1.** Refined lattice parameters and bond parameters of  $\text{Dy}_2\text{FeCoO}_6$  at 300 K, 150 K and 7 K. The nuclear structure was refined in orthorhombic  $Pnma$  space group. The atomic positions are Fe/Co at 4b (0, 0, 0.5), Dy at 4c ( $x$ , 0.25,  $z$ ), O at 8d ( $x$ ,  $y$ ,  $z$ ).

	300 K	150 K	7 K
$a$ (Å)	5.5056(2)	5.5026(2)	5.5031(8)
$b$ (Å)	7.5024(3)	7.4921(3)	7.4883(2)
$c$ (Å)	5.2390(2)	5.2333(2)	5.2333(7)
Fe/Co–O1	1.960(7)	1.957(7)	1.956(5)
Fe/Co–O2	1.988(5)	1.990(6)	1.990(5)
Fe/Co–O2	1.966(5)	1.976(5)	1.977(5)
Fe/Co–O1–Fe/Co	146.2(9)	146.1(9)	146.1(6)
Fe/Co–O2–Fe/Co	147.7(6)	146.2(6)	146.2(5)
$\chi^2$	2.35	1.60	1.43

$\Gamma_3(Gx, Ay, Fz)$ ,  $\Gamma_5(Cx, Fy, Az)$  and  $\Gamma_7(Fx, Cy, Gz)$ . Rietveld analysis of the 150 K data using the four different models suggested  $\Gamma_5(Cx, Fy, Az)$  as the best model to fit the experimental data. The fit using the combined nuclear and magnetic structures ( $Pnma + \Gamma_5(Cx, Fy, Az)$ ) is shown as black solid line in figure 4(a).

The magnetization data presented in figure 1(a) gives the evidence that  $\text{Dy}_2\text{FeCoO}_6$  undergoes a second magnetic transition at  $T_{\text{SR}} = 86$  K. Hence, the neutron diffraction data at 7 K must correspond to a possibly different magnetic structure after the spin reorientation has taken place. Figure 4(b) shows the Rietveld refined neutron diffraction pattern of  $\text{Dy}_2\text{FeCoO}_6$  at 7 K. The nuclear structure remains in the orthorhombic  $Pnma$  while the magnetic structure belongs to the representation  $\Gamma_3(Gx, Ay, Fz)$ . The temperature dependence of the (011) Bragg peak, shown in the inset of figure 4(b), follows an order parameter behaviour characterizing the spin reorientation transition at  $T_{\text{SR}}$ . The solid line in the figure is a fit using order parameter function to model the order parameter. A schematic of the magnetic structures of  $\text{Dy}_2\text{FeCoO}_6$  at 150 K and 7 K are presented as well in figure 4. The refined magnetic moment values are 1.07(3)  $\mu_B$  at 150 K and 1.47(4)  $\mu_B$  at 7 K. As a comparison, in the case of  $\text{La}_2\text{MnCoO}_6$ , both Mn and Co retained similar values of magnetic moment ( $\approx 2.4(2)$   $\mu_B$ ) at 10 K [45]. The refined lattice parameters, atomic coordinates and bond parameters of  $\text{Dy}_2\text{FeCoO}_6$  at 300 K, 150 K and 7 K are collected in table 1. The values of  $\chi^2$  signifying the goodness-of-fit are also given in the table.

#### 4.4. Density functional theory

We now present the details of the electronic and magnetic structures of  $\text{Dy}_2\text{FeCoO}_6$  obtained through DFT calculations. The total energy for different magnetic arrangements were calculated, namely ferromagnetic (FM), two antiferromagnets (AFM1 and AFM2) and three ferrimagnets (FIM1, FIM2 and FIM3), respectively. The experimental data in the temperature range, 7 K to 300 K suggests Dy to be not magnetically ordered. Based on this, the initial magnetic moment of Dy was set to zero, i.e., non-magnetic state, in DFT calculations. However, the final magnetic moment converged to strong magnetic character. Depending on the ordering of Fe

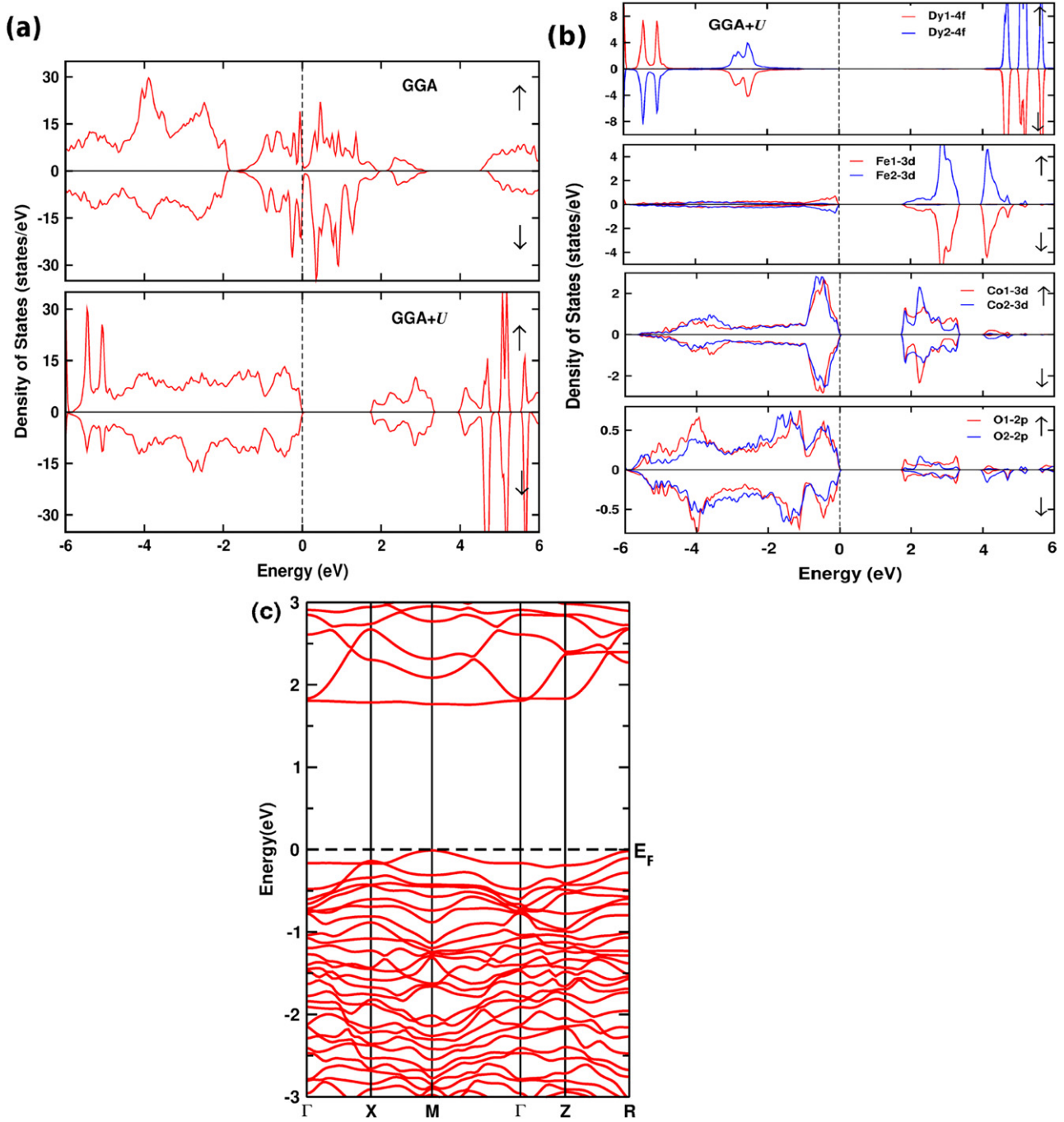


**Figure 5.** (a) Total DOS within GGA and GGA +  $U$  functional in spin up ( $\uparrow$ ) and spin down ( $\downarrow$ ) channel. The vertical dotted line indicates  $E_F = 0$ . (b) Partial DOS of Dy-4f, Fe-3d, Co-3d and O-2p in spin up ( $\uparrow$ ) and spin down ( $\downarrow$ ) channel. (c) Band structure within GGA +  $U$  functional.

and Co in  $\text{Dy}_2\text{FeCoO}_6$ , Dy moments arrange accordingly. Six magnetic configurations are generated by arranging magnetic atoms with up ( $\uparrow$ ) and down ( $\downarrow$ ) spins for four inequivalent atoms (Fe1, Fe2, Co1, Co2) as follows: FM- $\uparrow\uparrow\uparrow\uparrow$ , AFM1- $\uparrow\downarrow\downarrow\downarrow$ , AFM2- $\uparrow\downarrow\downarrow\uparrow$ , FIM1- $\uparrow\uparrow\downarrow\downarrow$ , FIM2- $\uparrow\downarrow\uparrow\uparrow$ , and FIM3- $\uparrow\uparrow\uparrow\downarrow$ . These arrangements have been considered in lowest space group  $P1$  which consists of four Dy, two each of Co and Fe, and twelve oxygen atoms in one chemical unit cell. By comparing the total energies of the six magnetic arrangements, AFM2 is the lowest total energy regardless of the

calculation scheme used. The energy difference to the next lowest order, AFM1, is small, viz, 10.4 meV/f.u. within GGA as shown in table S2 of the supplemental information (SI (<https://stacks.iop.org/JPCM/33/025802/mmedia>)). Small energy difference indicates a competing ground state between the AFM1 and AFM2 [24, 25]. Note that the effective moment of AFM2 is found to be  $10.0 \mu_B$ /unit cell which is due to the ferrimagnetic alignment of Dy atoms ( $\uparrow\uparrow\downarrow\downarrow$ ). While for AFM1 the effective moment becomes zero ( $0 \mu_B$ /unit cell) as four Dy atoms align antiferromagnetically with each other.



We start our investigation on the electronic structure of  $\text{Dy}_2\text{FeCoO}_6$  for the ground state AFM2 in scalar and full-relativistic mode both within GGA and GGA +  $U$  (electron-correlations effects,  $U = 7$  eV, 3 eV and 5 eV for Dy, Co and Fe, respectively). The spin-resolved total density of states (DOS) are shown in figure 5(a) for GGA and GGA +  $U$ . Within GGA, the material is found to be semi-metallic with small DOS at  $E_F$ . The main contributions around  $E_F$  are from the Dy-4*f*, Co-3*d*, and Fe-3*d* states (see figure S2 in SI). As seen from the partial DOS (see figure S2 of SI) for individual atoms, Co-3*d* are partially occupied by  $t_{2g}$  in spin-up and spin-down channel leaving the  $e_g$  states in the conduction band in both the spin channels. When compared, the amount of occupied contributions in spin-up is smaller ( $\sim 2$  electrons) as compared to the spin-down channel ( $\sim 3$  electrons). This indicates  $d^5$  configuration of Co where two electrons are occupied in spin-up and three in spin-down giving rise to a charge +4 (low-spin) state. When considering the individual Fe-atom, spin-up channel is fully occupied while only one state is occupied in spin-down channel resulting in  $d^6$  configuration with a charge state +2. This feature is found consistent with the individual moment in table 2. On the other hand, when  $U$  is applied, a band gap of  $\sim 1.77$  eV is noticed between the valence and conduction bands. The fully-occupied Dy-4*f* and Fe-3*d* states shifts deep in the valence region while the unoccupied state shifts to the conduction region giving rise to an insulating state. As observed in figure 5(b), the full occupancy of Dy-4*f* bands indicates the occupancy of 7 electrons in spin-up channel, while only two electron occupancy in spin-down channel resulting in  $\sim 5 \mu_B$  per Dy atom. The Fe-3*d* states are found prominent below  $-6$  eV hybridizing partly with Dy-4*f* and O-2*p* states, while Co-3*d* state hybridizes strongly with O-2*p* orbitals both in valence and the conduction region resulting in the charge-type insulator. One can notice the splitting of Co-3*d* bands into occupied  $t_{2g}$  in the valence region and an unoccupied  $e_g$  states above  $E_F$  in the conduction region for spin up channel. The partial DOS features of Co indicates the full occupancy of  $t_{2g}$  states in both the spin channels giving rise to low-spin with charge state  $\text{Co}^{3+}$  consistent with recent literature [13, 14]. The Fe-3*d* bands, on the other hand, are fully occupied by five electrons in spin-up and empty state in spin-down channel. This suggests a high-spin state of Fe with  $\text{Fe}^{3+}$  state consistent with our Mössbauer results based on the isomer shift values from the experiment. As per the band structure shown in figure 5(c), a direct band gap of  $\sim 1.77$  eV opens up at high symmetry point  $M$  due to electron-correlation dictating the insulating behavior of  $\text{Dy}_2\text{FeCoO}_6$ . It was not experimentally feasible to measure the resistance of the sample as a function of temperature due to large values  $\approx 10^8 \Omega$  at ambient temperatures. However, this value of resistance supports the picture of conduction emerging from our DFT calculations. It should be noted that with the increase in the  $U$  values of Co and Fe, the electronic band gap is found to rise for  $\text{Dy}_2\text{FeCoO}_6$  (see figure S7 of SI).

We can now consider the case of magnetism of Dy in  $\text{Dy}_2\text{FeCoO}_6$ . From the macroscopic magnetic experiments it turns out that Dy is not magnetically ordered down to 7 K. However, assuming the ionic picture, Dy nominally takes the

**Table 2.** Calculated spin magnetic moments (in  $\mu_B$ ) of Dy-4*f*, Fe-3*d*, Co-3*d* and band gap (in eV). The calculated orbital moments are shown within parentheses for  $\text{Dy}_2\text{FeCoO}_6$ .

	Dy	Fe	Co	Band gap (eV)
GGA	4.89	3.49	0.40	—
GGA + SOC	4.81	3.49	0.40	—
Orbital	(2.08)	(0.03)	(0.04)	
GGA + $U$	4.99	4.10	0.18	1.77
GGA + $U$ + SOC	4.97	4.10	0.18	1.73
Orbital	(1.98)	(0.01)	(0.02)	

charge state +3 with 4*f*<sup>9</sup> configuration in  $\text{Dy}_2\text{FeCoO}_6$ . This gives rise to a finite moment value of  $5 \mu_B$  per Dy atom. Our DFT calculation is in line with the ionic picture predicting a spin magnetic moment of  $4.99 \mu_B$  within GGA +  $U$ . To understand the magnetism without Dy, we generate an artificial material from  $\text{Dy}_2\text{FeCoO}_6$  where Dy is replaced with La atom. This results in the non-magnetism of the A-site atom. With this, we compute the ground state and hence the magnetic moment in Fe and Co, to see how much it is different from the values of that of  $\text{Dy}_2\text{FeCoO}_6$ . For the same, we start by searching for the magnetic ground state of  $\text{La}_2\text{FeCoO}_6$ , as that in  $\text{Dy}_2\text{FeCoO}_6$ . It is interesting to note that the replacement of Dy does not influence the magnetic ground state. i.e., AFM2 is found to be the ground state of the composition with an energy difference of 235.54 meV/f.u. compared to the AFM1 state as tabulated in table S2 of the supplemental information. This shows that with the inclusion of Dy, the value of total energy changes while the magnetic moments of Fe and Co do not change much (see table S1 of SI). The magnetic anisotropy energy (MAE) in  $\text{Dy}_2\text{FeCoO}_6$  is further investigated to check its influence on the electronic and magnetic properties. With an easy axis along the [111] direction, the computed MAE is 45 meV/unit cell within GGA.

## 5. Conclusions

We identify the double perovskite  $\text{Dy}_2\text{FeCoO}_6$  as an insulator with an antiferromagnetic transitions at 248 K and a spin reorientation transition at 86 K. The spin reorientation and the antiferromagnetic transitions at  $T_{SR} = 86$  K and  $T_N = 248$  K occurring in the Fe/Co sublattice are clearly brought out through the magnetization and neutron diffraction experiments on the current sample. The magnetic structure transforms from  $\Gamma_5(Cx, Fy, Az)$  to  $\Gamma_3(Gx, Ay, Fz)$  representation across the spin reorientation transition. DFT calculations support the experimentally determined magnetic features by predicting an antiferromagnetic AFM2 ground state which competes with comparable energies to AFM1; which are influenced by external magnetic fields. Our calculations converge to finite magnetism on the Dy site however, neutron diffraction experiments down to 7 K did not validate long-range magnetism in the Dy sublattice; which might order at still lower temperatures. An insulating ground state with a spin-gap of 1.77 eV emerges with the inclusion of electron correlation, thereby leading to a charge-type insulator. In conclusion,  $\text{Dy}_2\text{FeCoO}_6$  is identified as a rich magnetic system with an antiferromagnetic structure



showing spin reorientation transition and an insulating state. Our study opens the possibility to investigate  $\text{Dy}_2\text{FeCoO}_6$  further as an insulating system with emerging physics in the strongly correlated regime.

## Acknowledgments

HSN acknowledges faculty start-up funds from UTEP and Rising STAR award from University of Texas. GRH thanks Dr Raghavendra Reddy (UGC CSR Indore) for Mössbauer measurement at 300 K and Dr Shibnath Samanta for the help received during sample synthesis. GRH, PR, KS and VSN acknowledge IITM for funding provided for SVSM. MPG thanks the Alexander von Humboldt Foundation for financial support, and the Higher Education Reform Project (HERP DLI-7B) of Tribhuvan University, Kirtipur, Nepal for start-up grant. PV and JJ acknowledge support from the National Science Foundation under Grant No. DMR-1748650 and the George Mason University Quantum Materials Center.

## ORCID iDs

G R Haripriya  <https://orcid.org/0000-0002-2888-6910>  
 Madhav Prasad Ghimire  <https://orcid.org/0000-0003-2783-4008>

P Vora  <https://orcid.org/0000-0003-3967-8137>

K Sethupathi  <https://orcid.org/0000-0002-2948-4737>

V Sankaranarayanan  <https://orcid.org/0000-0002-9481-4237>

H S Nair  <https://orcid.org/0000-0002-4301-9380>

## References

- [1] Yáñez Vilar S *et al* 2011 *Phys. Rev. B* **84** 134427
- [2] Shimakawa Y, Azuma M and Ichikawa N 2011 *Materials* **4** 153–68
- [3] Witczak-Krempa W, Chen G, Kim Y B and Balents L 2014 *Annu. Rev. Condens. Matter Phys.* **5** 57–82
- [4] Huang Y H, Dass R I, Xing Z L and Goodenough J B 2006 *Science* **312** 254–7
- [5] Kobayashi K I, Kimura T, Sawada H, Terakura K and Tokura Y 1998 *Nature* **395** 677–80
- [6] Cavichini A, Orlando M, Depianti J, Passamai J Jr, Damay F, Porcher F and Granado E 2018 *Phys. Rev. B* **97** 054431
- [7] Chen H and Millis A 2017 *Sci. Rep.* **7** 6142
- [8] Tokunaga Y, Iguchi S, Arima T and Tokura Y 2008 *Phys. Rev. Lett.* **101** 097205
- [9] Stroppa A, Marsman M, Kresse G and Picozzi S 2010 *New J. Phys.* **12** 093026
- [10] Knížek K, Jiráček Z, Novák P and de la Cruz C 2014 *Solid State Sci.* **28** 26–30
- [11] Knížek K, Jiráček Z, Hejtmanek J, Veverka M, Maryško M, Maris G and Palstra T 2005 *Europhys. J. B* **47** 213–20
- [12] Karpinsky D V, Troyanchuk I O, Bärner K, Szymczak H and Tovar M 2005 *J. Phys.: Condens. Matter* **17** 7219
- [13] Fuh H R, Weng K C, Chang C R and Wang Y K 2015 *J. Appl. Phys.* **117** 17B902
- [14] Fuh H R, Weng K C, Liu Y P and Wang Y K 2015 *J. Alloys Compd.* **622** 657–61
- [15] Haripriya G R, Pradheesh R, Singh M N, Sinha A K, Sethupathi K and Sankaranarayanan V 2017 *AIP Adv.* **7** 055826
- [16] Rietveld H M 1969 *J. Appl. Crystallogr.* **2** 65–71
- [17] Rodriguez-Carvajal J 2017 Fullprof Suite (<http://www.ill.eu/sites/fullprof/>)
- [18] Wills A S 2000 *Physica B* **276** 680–1
- [19] Momma K and Izumi F 2011 *J. Appl. Crystallogr.* **44** 1272–6
- [20] Blaha P, Schwarz K, Madsen G, Kvasnicka D and Luitz J 2001 WIEN2k An Augmented Plane Wave Plus Local Orbitals Program for Calculating Crystal Properties (<http://www.wien2k.at>)
- [21] Perdew J P, Burke K and Ernzerhof M 1996 *Phys. Rev. Lett.* **77** 3865
- [22] Anisimov V I, Poteryaev A I, Korotin M A, Anokhin A O and Kotliar G 1997 *J. Phys.: Condens. Matter* **9** 7359
- [23] Ghimire M P, Wu L and Hu X 2016 *Phys. Rev. B* **93** 134421
- [24] Yuan Y, Feng H L, Ghimire M P, Matsushita Y, Tsujimoto Y, He J, Tanaka M, Katsuya Y and Yamaura K 2015 *Inorg. Chem.* **54** 3422–31
- [25] Feng H L *et al* 2016 *Phys. Rev. B* **94** 235158
- [26] Ghimire M P, Thapa R K, Rai D P, Sandeep, Sinha T P and Hu X 2015 *J. Appl. Phys.* **117** 063903
- [27] Ghimire M P and Hu X 2016 *Mater. Res. Express* **3** 106107
- [28] Ghimire M P, Sandeep C, Sinha T P and Thapa R K 2011 *Solid State Commun.* **151** 1224–7
- [29] Mali B, Nair H S, Heitmann T, Nhalil H, Antonio D, Gofryk K, Bhandari S R, Ghimire M P and Elizabeth S 2020 *Phys. Rev. B* **102** 014418
- [30] Kuneš J, Novak P, Schmid R, Blaha P and Schwarz K 2001 *Phys. Rev. B* **64** 153102
- [31] Zhou Z, Guo L, Yang H, Liu Q and Ye F 2014 *J. Alloys Compd.* **583** 21–31
- [32] Haripriya G R, Pradheesh R, Sethupathi K and Sankaranarayanan V 2018 *AIP Adv.* **8** 101340
- [33] Hjøllum J *Fit ;o)—A Mössbauer spectrum fitting program* (<https://hjolium.com/jari/zzbug/fit/>)
- [34] Liang Y, Di N and Cheng Z 2006 *J. Magn. Magn. Mater.* **306** 35–9
- [35] Ganesanpotti S, Tassel C, Hayashi N, Goto Y, Bouilly G, Yajima T, Kobayashi Y and Kageyama H 2014 *Eur. J. Inorg. Chem.* **2014** 2576–81
- [36] Uhm Y R, Kim S J and Kim C S 2002 *J. Magn.* **7** 18–20
- [37] Weber M C, Guennou M, Zhao H J, Íñiguez J, Vilarinho R, Almeida A, Moreira J A and Kreisel J 2016 *Phys. Rev. B* **94** 214103
- [38] Wei-Ran W, Da-Peng X, Wen-Hui S, Zhan-Hui D, Yan-Feng X and Geng-Xin S 2005 *Chin. Phys. Lett.* **22** 2400
- [39] Weber M C, Kreisel J, Thomas P A, Newton M, Sardar K and Walton R I 2012 *Phys. Rev. B* **85** 054303
- [40] Andreasson J, Holmlund J, Knee C S, Käll M, Börjesson L, Naler S, Bäckström J, Rübhausen M, Azad A K, and Eriksson S G 2007 *Phys. Rev. B* **75** 104302
- [41] Kotnana G, Sathe V G and Jammalamadaka S N 2018 *J. Raman Spectrosc.* **49** 764–70
- [42] Yin L H, Yang J, Zhang R R, Dai J M, Song W H and Sun Y P 2014 *Appl. Phys. Lett.* **104** 032904
- [43] Yuan B, Yang J, Zuo X Z, Kan X C, Zhu X B, Dai J M, Song W H and Sun Y P 2016 *J. Alloys Compd.* **656** 830–4
- [44] Kotnana G and Jammalamadaka S N 2015 *J. Appl. Phys.* **118** 124101
- [45] Barón-González A, Frontera C, García-Muñoz J L, Rivas-Murias B and Blasco J 2011 *J. Phys.: Condens. Matter* **23** 496003